DOI: 10.2478/fas-2022-0009
FATIGUE OF AIRCRAFT STRUCTURES
Volume 2022: Issue 14, pp. 114-134

COMPARATIVE ANALYSIS OF THE LOAD SPECTRA RECORDED DURING PHOTOGRAMMETRIC MISSIONS OF LIGHTWEIGHT UAVS IN TAILLESS AND CONVENTIONAL CONFIGURATIONS

Rodzewicz Mirosław[1*], Głowacki Dominik[1], Hajduk Jarosław[2]
[1]Warsaw University of Technology, Institute of Aeronautics and Applied Mechanics, Nowowiejska 24, 00-665 Warsaw,Poland
[2]Air Force Institute of Technology, Księcia Bolesława 6, 01-494 Warsaw, Poland

miroslaw.rodzewicz@pw.edu.pl

Abstract

The purpose of this article is to present the results of the investigation regarding the differences of the load spectra of two unmanned fixed-wing aircraft performing photogrammetry missions: X-8 (flying wing) and PW-ZOOM (conventional configuration). The focus was on the analysis of a number of load cycles for various load increments within the range of the operational loads. The load spectra were determined using the acceleration signal recorded in the autopilot logs as an input. This signal was transferred to the chain of local extreme values scaled in the form of discrete load levels, and then the transfer arrays were derived with use of the rainflow counting algorithm. On this basis, the incremental load spectra were determined for each flight. These load spectra were subjected to statistical analyses to determine the load spectra representative of the flight sessions in a few ways between non-conservative (i.e., focused on average load histories) and conservative (i.e., focused on the worst load histories observed during the flight session). Finally, the fatigue life was calculated by having the structural element of the assumed fatigue properties subjected to the load spectra of both airplanes. A large (exceeding one order of magnitude) difference in the number of load cycles for larger load increments in the analyzed load spectra was shown. This difference is related to the different dynamic characteristics of the two aircraft, in particular the gust response. As a result, there is a several-fold difference in fatigue life.

Keywords: load spectra, fatigue life, unmanned aircraft, photogrammetry mission
Article Category: research article

Nomenclature – main symbols and abbreviations

aggregated LS – average load spectrum of the whole flight session
ILS – incremental load spectrum; (ILSs – *plural form*)
LS – load spectrum; (LSs – *plural form*)
LS envelope – an envelope of the load spectrum of the whole flight session
n_C – cumulated number of load cycles (i.e., summarized number of load cycles from the current value of ΔLL up to the highest one)
n_1hC – cumulated number of load cycles related to 1 h of flight
n_L – level number of load cycles (i.e., number of load cycles for current value of ΔLL)
n_1hL – exact value of load cycles for given ΔLL related to 1 h of flight
$n_1hL_{j,f}$ – the element of the **n_1hL array,** where j is the ΔLL value and f is an index of the flight
n_1hL_agg, n_1hC_agg – the level and cumulative values of the aggregated LS
n_1hL_env, n_1hC_env – the level and cumulative values of the LS envelope
n_1hL_wenv, n_1hC_wenv – the level and the cumulative values of LS-weighted envelope
$n_1hL_m{+}1s$, $n_1hC_m{+}1s$ – the level and cumulative values of the LS
n_z – load factor
n_{z_max} and n_{z_min} – extreme operating load limits
Δn_z – load factor increment
LL – load level (load represented as integer number in 32-step scale covering the operational load range)
ΔLL – load level increment, when the load signal transfers to the next local extremum
t – time, t_f – time of the f-indexed flight, t_T – total time of the whole flight session

Introduction

A significant increase in the use of unmanned aerial vehicles (UAVs) is observed in various fields of the civil economy; see: (Everaerts, 2008; Norasma et al., 2019; Giordan et al., 2020; Goetzendorf-Grabowski et al., 2021; Zmarz et al., 2018, as well as in the military field (Slack, 2013; Kozera, 2018). The joint use of airspace by manned and unmanned aviation makes the safety issues of the UAV operations a major problem. One of the important aspects is reliability, especially in terms of structural strength and fatigue life (Jin et al., 2013; Rodzewicz, 2012). To estimate the fatigue life, it is necessary to know the load spectra. For this reason, it is important to investigate the load spectra of various types of UAVs. It is well known that the loads in flight depend on the dynamic characteristics of aircraft, the type of maneuvers performed, and air turbulence (Leishman, 2022; Rodzewicz and Glowacki, 2020). The dynamic characteristics of the plane mainly depend on the adopted aerodynamic configuration and airframe geometry, mass characteristics, and characteristics of the installed propulsion systems. However, the behavior of the UAV in the air is the result of the entire system operation, including the aircraft and the autopilot. Both of them must be mutually integrated (in the sense of adjusting the dynamic characteristics of both subsystems), and this applies to an automatic flight in particular. It has already been

investigated that the load spectrum (LS) in automatic flight differs from that of remote manual control (Glowacki and Rodzewicz, 2014). This is due to the fact that the UAV operator is deprived of stimuli in the form of feeling the acceleration, so the operator reacts mainly by observing the change in the aircraft's position in space (i.e., the effect of integration of these accelerations over the time). Due to the lack of acceleration sensing by the UAV operator, the spectrum of loads with manual control is therefore more aggressive and causes a greater fatigue effect.

The mild spectrum of loads is associated with a calm flight and a smooth flight path. This is very important when a UAV performs a photogrammetric mission. This is both about the quality of the photos, which must not be blurred, and about keeping the axis of the camera vertical with a very small tolerance for deviations. This is especially important when the aircraft is not equipped with stabilization systems for the optical axis of the camera (Rodzewicz et al., 2017). In small planes, this is not always possible because the photogrammetry camera itself is a large load that exhausts the loading capacity of the plane. This was the case with the UAVs described in this article.

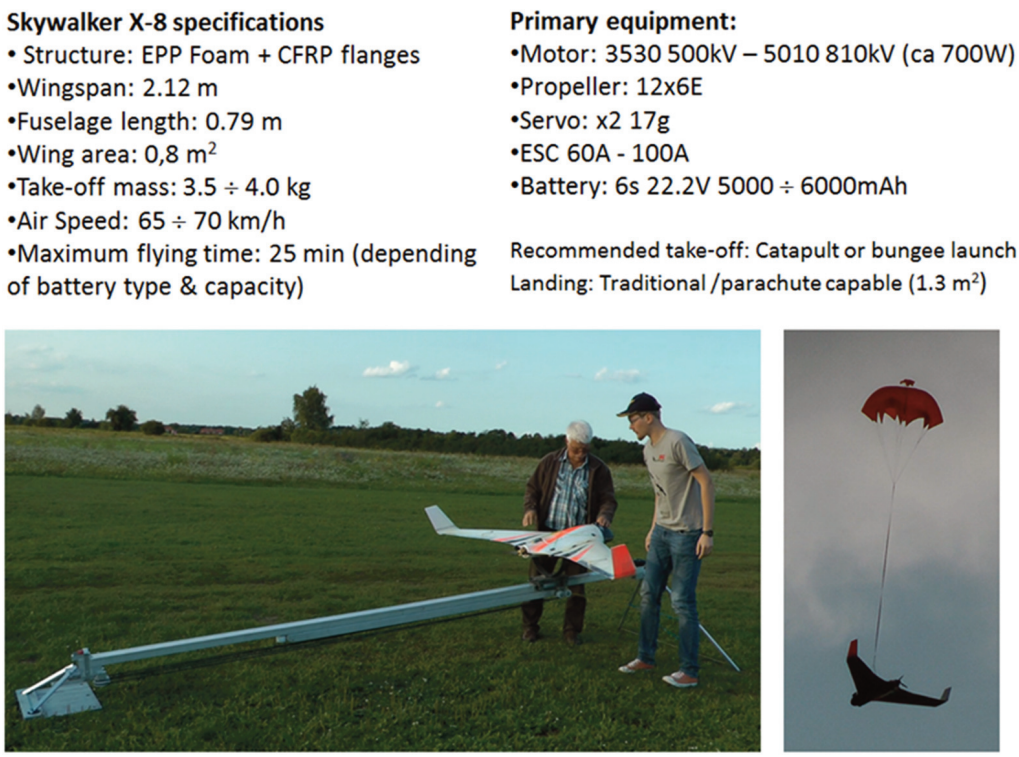
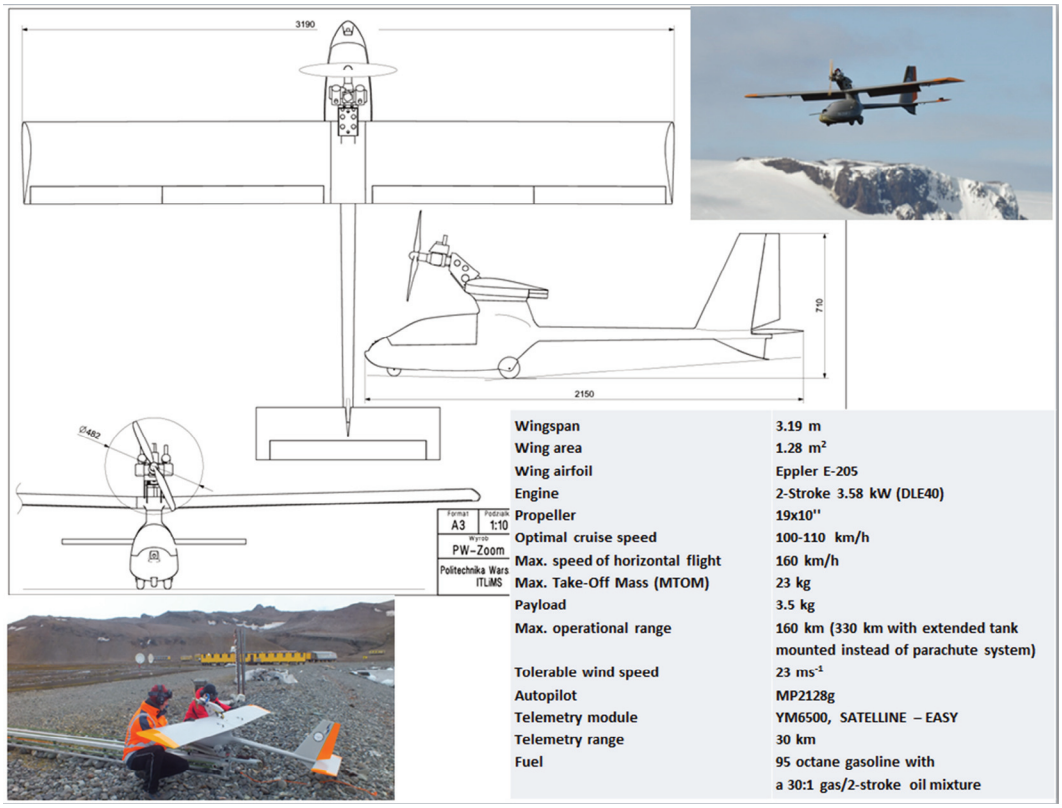


Figure 1. Data of the X-8 flying wing and the planes used by the authors' team for experiments.

The purpose of this work is to study the differences between the load spectra of two lightweight unmanned vehicles of different aerodynamic designs (flying wing vs conventional configuration) that were used by the authors for photogrammetry missions (Zmarz et al., 2018). One of them is the popular flying wing X-8, for which kits are available on the market (Gryte et al. 2018). The other UAV is the PW-ZOOM – the plane designed and used for monitoring Antarctic areas (Goetzenderf-Grabowski

and Rodzewicz, 2017). Although both aircraft differ from each other in terms of aerodynamics and structure, they belong to the same UAV class (having MTOM 25 kg).The data of both planes are shown in Figs. 1 and 2.



Wingspan	3.19 m
Wing area	1.28 m^2
Wing airfoil	Eppler E-205
Engine	2-Stroke 3.58 kW (DLE40)
Propeller	19x10''
Optimal cruise speed	100-110 km/h
Max. speed of horizontal flight	160 km/h
Max. Take-Off Mass (MTOM)	23 kg
Payload	3.5 kg
Max. operational range	160 km (330 km with extended tank mounted instead of parachute system)
Tolerable wind speed	23 ms^{-1}
Autopilot	MP2128g
Telemetry module	YM6500, SATELLINE – EASY
Telemetry range	30 km
Fuel	95 octane gasoline with a 30:1 gas/2-stroke oil mixture

Figure 2. Technical data of the PW-ZOOM.

The differences between these two aircraft are easy to see, but what they have in common is the same photogrammetry equipment (i.e., Canon 700D camera with the GPS) and the same type of autopilot (i.e., Micropilot MP2128g). Due to the different performance levels of the two aircraft, the X-8 aircraft is used for short-range photogrammetric missions (up to 30 km), while the PW-ZOOM aircraft is used for the missions up to 330 km.

The presence on board of the MP2118g autopilot allows us to record several dozen flight parameters, including servos positions, airspeed, GPS speed, GPS position, altitude, heading, current pitch and roll, 3-axis data concerning linear and angle accelerations. All these data are stored in the autopilot memory as a log-file with the specific sampling frequency (here it was 5 Hz). This source of data allows many analyses, especially those concerning the dynamic behavior of planes and the LS, which is the focus of this study.

The signal that is necessary for the LS analysis is a_z (i.e., acceleration along the *z* design axis, which is oriented vertically during a normal horizontal flight). On this basis, the load factor n_z is calculated, as shown in Eq. (1):

$$n_z(t) = \frac{a_z(t)}{g}, \quad \text{where } g \text{ is the Earth acceleration and } t \text{ is time} \tag{1}$$

The load signal $n_z(t)$ representing a string of real numbers is then transformed into a string of discrete load levels LL(t). As a standard, 32 load levels are applied, following a standardization formula similar to that used for composite gliders or light composite airplanes (Kossira and Reinke, 1986):

$$LL = 3 \text{ for } n_{z_max} \text{ and } LL = 31 \text{ for } n_{z_min}; \quad (2)$$

The interval LL = 3 up to LL = 31 represents the operational load range, and the n_{z_max} and n_{z_min} are extreme operating load limits. The LL = 1, 2, and 32 are reserved for the cases of incidental overloading of the aircraft beyond the operational limit.

The 3rd step of load signal elaboration consists in filtering the signal to the form local extremes chain (see Figure 3). The chain of local extremes becomes an input to the process based on the rainflow counting algorithm. The output of this process is a transfer array named the half cycle array (HC array) or full cycle array (depending on an applied algorithm (Rodzewicz, 2023).

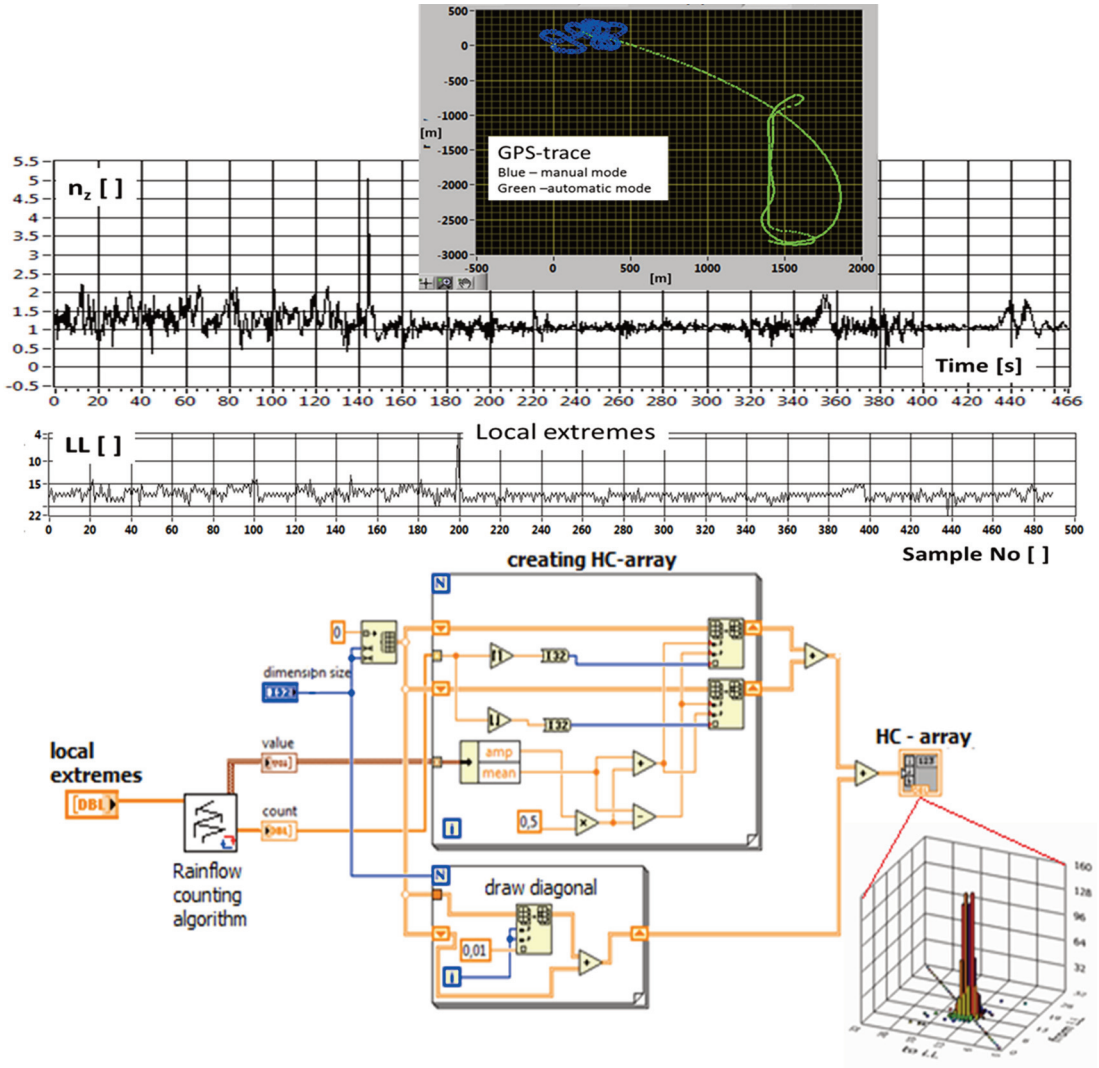


Figure 3. Schema of load signal processing and derivation of the HC array.

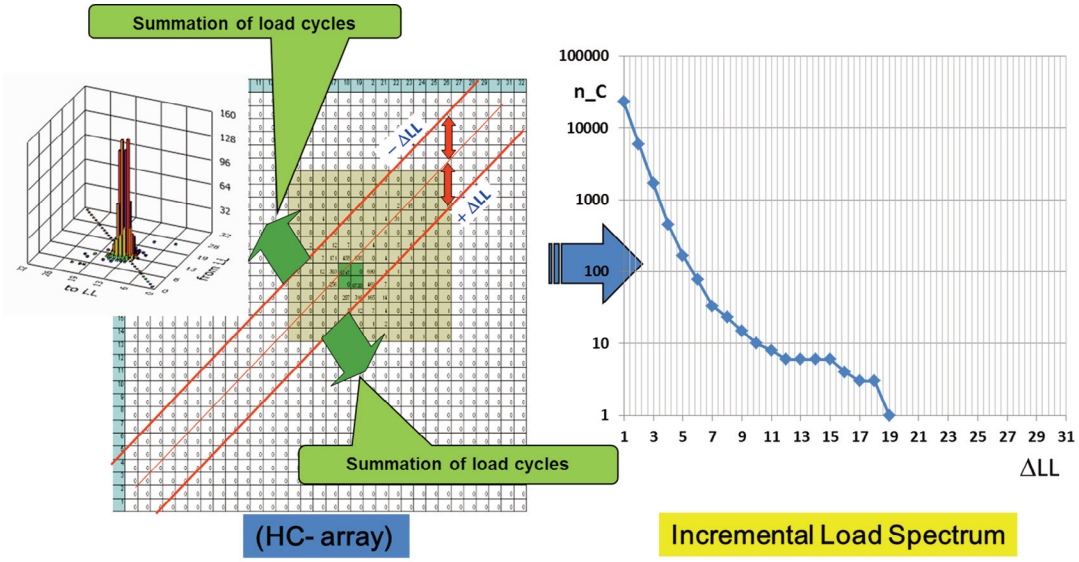


Figure 4. Schema of the incremental load spectrum derivation process.

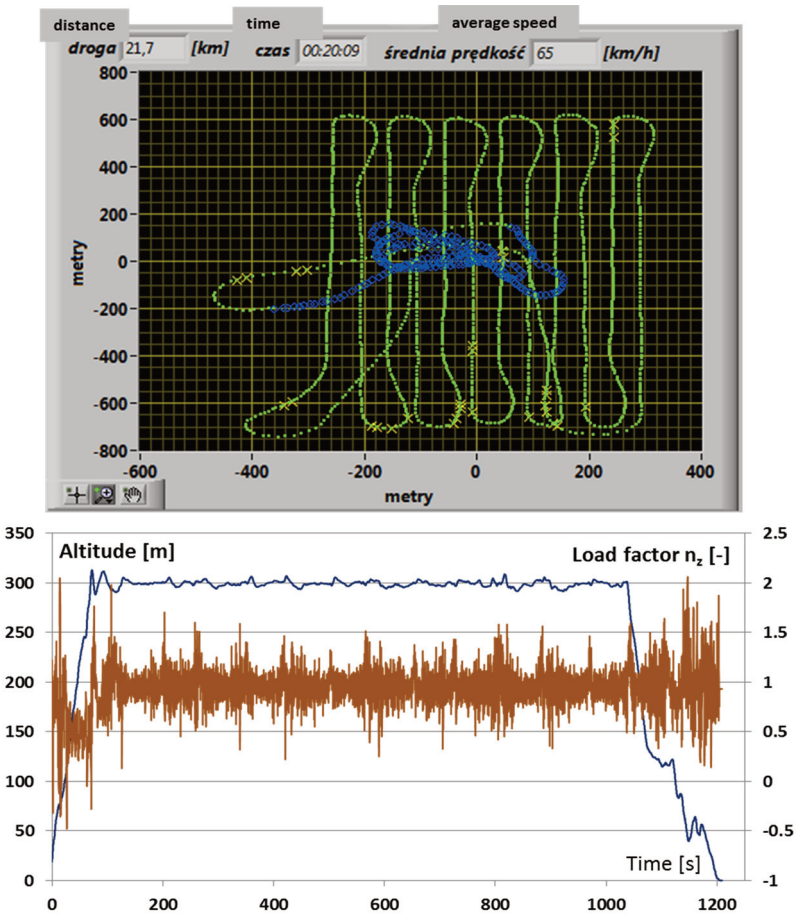


Figure 5. Illustration of the main flight data of the X-8 stored in the file log20151010_125213.

With the HC array, it is possible to derive the incremental load spectrum in the form of a chart with the values of load increments ΔLL on the horizontal axis and a cumulated number of load cycles *n_C* on the vertical axis (Fig. 4). The expression "cumulated" means that it is a sum of load cycles for ΔLL equal to or higher than a concerned value; for example, the number of load cycles for ΔLL = 1 is a sum of load cycles of all possible load increments. According to the standardization formula, the maximum value of ΔLL within the operational load limit is theoretically equal to 28, but usually during photogrammetry flights (which have to be very stable), the load increments are not so high.

The entire signal processing process was carried out by the authors through a program written in the LabView environment.

The example of the result concerning X-8 flight data recorded as a file log20151010_125213 is shown in Figs. 5 and 6. Figure 5 contains the GPS trajectory of the flight. The green path denotes automatic control, while the blue path denotes the manual control during the take-off and landing. The chart shows the load signal and the altitude (which is added for better illustration of the course of the flight).

Flight log:	log20151010_125213		Flight time	0.335833
ΔLL [-]	n_C [-]	n_L [-]	n_1hC [1/h]	n_1hL [1/h]
1	2929	2099	8721.588	6250.124
2	830	634	2471.464	1887.841
3	196	134	583.6228	399.0074
4	62	36	184.6154	107.196
5	26	12	77.41935	35.73201
6	14	8	41.68734	23.82134
7	6	3	17.866	8.933002
8	3	0	8.933002	0
9	3	3	8.933002	8.933002
10	0	0	0	0
11	0	0	0	0
12	0	0	0	0
13	0	0	0	0
14	0	0	0	0
15	0	0	0	0
16	0	0	0	0
17	0	0	0	0
18	0	0	0	0
19	0	0	0	0
20	0	0	0	0
21	0	0	0	0
22	0	0	0	0
23	0	0	0	0
24	0	0	0	0
25	0	0	0	0
26	0	0	0	0
27	0	0	0	0
28	0	0	0	0

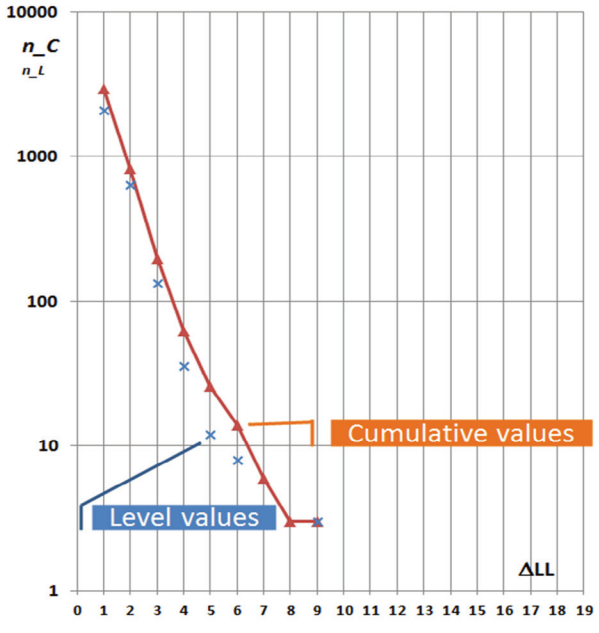


Figure 6. Results of load signal elaboration of log20151010_125213: the incremental load spectra.

Figure 6 shows the cumulated number of load cycles *n_C* and the level number of load cycles *n_L* (representing the absolute data of load cycles for the current ΔLL value), as well as the same data but related to 1 h of flight: *n_1hC* and *n_1hL*. The chart in Fig. 6 presents the incremental load spectra (ILSs): *n_C* and *n_L* vs ΔLL.

Analysis of the Load Spectra

Several analyses of the load spectra which occurred during photogrammetry flights of both UAVs: X-8 and PW-ZOOM – are described in this section. As the authors had 10 logs of X-8 flights and 23 logs of PW-ZOOM flights at their disposal – it was decided to use two approaches for PW-ZOOM logs analysis: at first, dealing only with 10 logs from the selected flights, and then dealing with all the 23 logs. The selected 10 logs concern PW-ZOOM flights performed in conditions similar to the X-8 operation conditions (good weather with stable wind up to 5 m/s without thermal gusts, conducive to generating a moderate LS).

Another aspect that was taken into account was a way of UAV control because automated control and manual control produce different LSs (Glowacki and Rodzewicz, 2013). Therefore, all analyses were conducted twice: for entire flights (covering manual control during the take-off and landing) and the part of the flights controlled by autopilot while flying along the programmed photogrammetric route using only the automated mode. All analyses are listed in Table 1.

Table 1. LS analysis cases

X-8 load spectra of entire photogrammetry flights (manual control and automatic control – 10 flights, total time: 3.047 h)	PW-ZOOM load spectra of entire photogrammetry flights (manual control and automatic control – 10 flights, total time: 12.935 h)
	PW-ZOOM load spectra only for the photogrammetric part (automatic control – the same 10 flights, total time: 10.957 h)
X-8 load spectra only for the photogrammetric part (automatic control – the same 10 flights, total time: 2.440 h)	PW-ZOOM load spectra of entire photogrammetry flights (manual control and automatic control – 23 flights; total time: 30.072 h)
	PW-ZOOM load spectra only for the photogrammetric part (automatic control – the same 23 flights, total time: 24.961 h)

To be able to compare the load spectra of both UAVs, the following parameters for the standardization formula were considered:

$$LL = 3 \text{ for } n_Z = 5 \text{ and } LL = 31 \text{ for } n_Z = -3; \quad (2a)$$

It was checked before that this range of n_Z variation is sufficient enough for both the X-8 and the PW-ZOOM load spectra regardless of the control mode and flight conditions.

The process of LS analysis will be explained using as an example 10 logs covering the entire flights of X-8. All the 10 flights were made at 300 m AGL over the same flat

terrain in the aforementioned non-turbulent weather conditions. In the case of the analyzed logs for the entire 10 flights of X-8, the range of maximum ΔLL value variation was $6 \leq \Delta LL\ 19$.

Basing on Eq. (2a), the incremental load spectra were derived for all the 10 flights and presented in the form of tables and charts (n_1hC and n_1hL vs ΔLL) in the same manner as the one described in Fig. 6. Next, two arrays were created in Excel. The 1st array was the **n_1hL array**, which contains 19 rows (each for a certain value of ΔLL) and 10 columns with the LS data (each for a certain flight). An element of this array was labeled as $n_1hL_{j,f}$, where j is the number of rows (i.e., ΔLL values) and f is an index of the flight (i.e., column number).

The 2nd array was the 1-row **t array**, which contains all the flight times. An element of this array was labeled as t_f. This array is of an auxiliary nature in performed calculations.

Load spectra analysis

The database described previously allows starting the analysis of the LS for the entire flight session (i.e., covering several flights) taking different aspects into account.

A/ The aggregated LS

The analysis can start by determining the aggregated LS. To do this, it is necessary to sum level values n_L of absolute data of load cycles for a particular value of ΔLL, and then to divide it by the total time of all flights, to obtain n_1hL values. Then, the cumulated values n_1hC are determined by integrating the n_1hL values starting from the highest ΔLL.

Example: for ΔLL=*j:*

$$n_1hL_agg_j = \sum_{f=1}^{F}\left(n_L_{j,f}\right)\Big/t_T = \sum_{f=1}^{F}\left(n_1hL_{j,f}\cdot t_f\right)\Big/t_T \ ; \tag{3}$$

$$n_1hC_agg_j = \sum_{j=j}^{j} n_1hL_agg_j \ ; \tag{4}$$

where j = 1,2, .., J and f=1,2,..,F;

In the case of the aggregated LS from the X-8 flight session covering 10 flights during which the maximum load increment value was ΔLL = 19. The values of F and J parameters are as follows: F = 10 and J = 19. The total time of all flights t_T = 12,935 h.

B/ LS envelope

To create the LS envelope, it is necessary to find maxima in each column of the **n_1hL array** (i.e., to find the maxima of $n_1hL_{j,f}$ for each particular j-value). This process for ΔLL = j is described by Eqs (5) and (6).

$$n_1hL_env_j = MAX_{f=1}^{F}\left(n_1hL_{j,f}\right); \tag{5}$$

$$n_1hC_env_j = \sum_{j=J}^{j}\left(n_1hL_env_j\right); \tag{6}$$

The results of calculation for the aggregated LS and the LS envelope (together with 10 ILSs from the X-8 flights) are presented in Fig. 7. The aggregated LS represents the values averaged for the whole flight session. Such LS is non-conservative because almost half of flights indicate a higher number of load cycles for particular ΔLL values in comparison with the aggregated LS. Using the aggregated LS for fatigue life calculations will result in a high risk of overestimating the result. On the other hand, the LS envelope gives conservative results because it represents the extreme values of n_1hL that occurred during the whole flight session. The chart shows that number of load cycles per 1 h differs for both curves of about 1 order for the most ΔLL values.

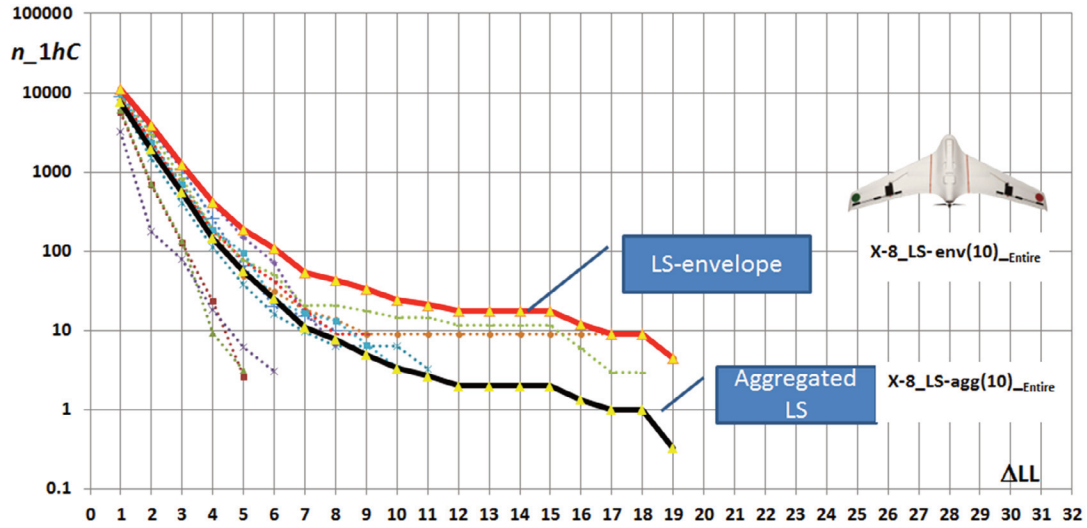


Figure 7. Incremental load spectra of all 10 X-8 flights (dotted lines) and the aggregated LS and LS envelope for the whole flight session.

All curves in Fig. 7 refer to the entire flights from the take-off to landing without distinguishing between the manual and automatic controlled flight fragments.

C/ Load spectra statistical analysis – equal or weighted influence of the flights

To assess the conservatism of the LS represented by the LS envelope, the load spectra based on the mean value plus 1, 2, or 3 standard deviations were examined. They were created by calculating the mean value and standard deviation (function symbols in the text: MEAN and STD) for each row of the **n_1hL array.**

The following example shows the procedure for the case "mean value plus 1 standard deviation" (indexed as "m+1s"). The operations are described by formulas (7) and (8):

For each ΔLL = *j*,

$$n_1hL_m+1s_j = MEAN\left(n_1hL_{j,f}\right) + STD\left(n_1hL_{j,f}\right); \tag{7}$$

$$n_1hC_m+1s_j = \sum_{j=J}^{j}\left(n_1hL_m+1s_j\right); \tag{8}$$

Note: To create such the LSs, an assumption was made that if the series of $n_1hL_{j,f}$ values for the chosen index j contains only single non-zero data, then the sum of the mean value plus 1, 2, or 3 standard deviation will be equal to the value of the non-zero data.

The aforementioned approach assumes that each flight, regardless of its duration, has the same impact on the LS representative for the whole flight session.

In the next approach, the authors decided to check the case when the impact of each flight will depend on the time share in the entire flight session. The time-shares of all flights were summed for each ΔLL and used as the "weight coefficients" to generate the weighted load spectra representing mean plus 1, 2, or 3 standard deviations or representing an LS-weighted envelope.

The "weight coefficient" is applied to each ΔLL step and is defined by the following formula (9):

For ΔLL=j,

$$w_j = \sum_{f=1}^{F} \mathrm{sgn}\left(n_1hL_{j,f}\right) * t_f / t_T \,. \tag{9}$$

The **sgn** function takes the value 0 or 1 depending on whether at least one load cycle occurred for a given ΔLL = j in flight f.

In the case of the LS-weighted envelope, the formulas (5) and (6) are modified.

Example: for ΔLL = j,

$$n_1hL_wenv_j = MAX_{f=1}^{F}\left(n_1hL_{j,f}\right) * w_j; \tag{5a}$$

$$n_1hC_wenv_j = \sum_{j=J}^{j}\left(n_1hL_wenv_j\right); \tag{6a}$$

where, j is an index related to ΔLL value and f is an index of the flight.

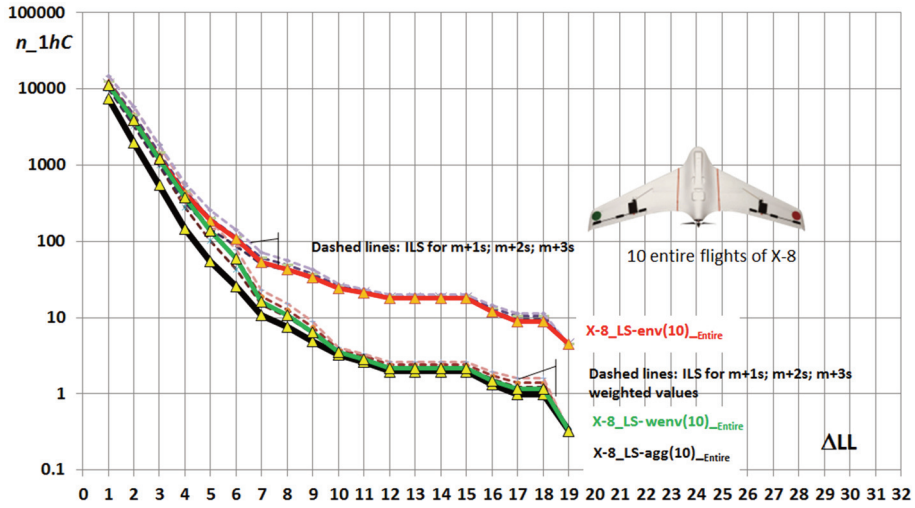


Figure 8. Chart representing the ILS based on the MEAN and STD of n_1hL values, and the ILS for the LS envelope and the LS-weighted envelope.

In the same manner, the formulas for the load spectra representing the weighted values of mean value plus 1, 2, or 3 standard deviations were also modified.

The results of both approaches are presented in Fig. 8.

As one can see, the difference between the direct and weighted n_1hC values depends on the ΔLL and exceeds one order for higher ΔLL values. According to the P-M hypothesis, it may significantly influence the calculated value of fatigue life. The graph also shows that the LS envelope gives the results located between the lines corresponding to m+1s and m+3s – both for ILSs based on the direct and weighted values of $n_1hL_{j,f}$. This shows that instead of using the MEAN and STD functions, it is better to use the LS envelope procedure as it produces similar results, and there is no need for an exception for the case where there is only a single indication in the dataset for a given ΔLL.

The LS-weighted envelope lies in the entire range of ΔLL above aggregated LS, but for large values of n_1hC (above 200 load cycles/h corresponding to ΔLL<5), it coincides with LS envelope, while for small values of n_1hC (below 3 load cycles/h corresponding to ΔLL>10), it is very close to the aggregated LS.

Such a position of the curves means that the probability that n_1hC will exceed the value represented by LS envelope is small* in the range of coincidences with the LS-weighted envelope, and large* in the range where the LS-weighted envelope is close to the aggregated LS. This conclusion can be proved by the chart presented in the next section (Fig. 9) showing the development of both LS envelopes when the number of flights increases.

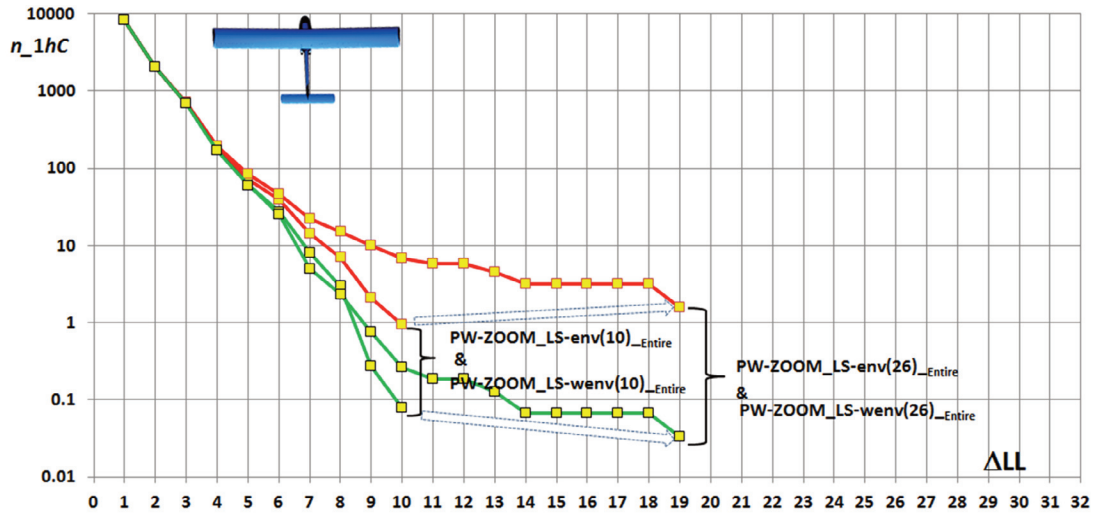


Figure 9. Impact of the increase in the number of flights and the resulting total time on the LS represented by normal and weighted envelopes.

* *NOTE*: a small or large probability means the range of variation from about 0.1 up to 0.5, but these numbers refer to the case where we would deal with a semi-Gaussian distribution of n_1hL values for a given ΔLL. Currently, the use of this statistical model is unjustified due to too small a database.

Considering the LS representative for the flight session, and knowing that the LS envelope represents the conservative LS, while the aggregated LS represents the non-conservative LS, we can conclude that the LS-weighted envelope represents the semi-conservative LS.

Preliminary analysis of the PW-ZOOM LS – a test of the developed method of analyzing load spectra in the case of the PW-ZOOM

Before proceeding to a full comparative analysis of the load spectra of both UAVs, preliminary analyses of the PW-ZOOM's load spectra were performed. Because the X-8 was operated in conditions of moderate turbulence, 10 PW-ZOOM flights performed under similar conditions were selected. During those analyses, it was fully confirmed that all calculation methods used for the X-8 produced similar dependencies in the case of PW-ZOOM as well. The main difference that was found is only the range of variability for ΔLL and n_1hL values. In comparison with the X-8, the maximum ΔLL value for PW-ZOOM is about 50% lower. Also, the number of load cycles for higher ΔLL values is much lower. Generally, this means that PW-ZOOM's flights in similar flight conditions are much calmer than those in the case of X-8 (fewer oscillations of n_Z value). For this reason, for further comparative analysis, it was decided to take all PW-ZOOM flights into account – regardless of weather conditions, because the PW-ZOOM's load range will be more similar to that of the X-8. The effect of this decision is presented in Fig. 9 in the form of the LS envelopes: normal and weighted. One can see that both the range of load variation and the number of load cycles for higher ΔLL values increased significantly for the flight session covering all the 26 flights.

Comparative analysis of X-8 and PW-ZOOM photogrammetry flights

Comparison of the X-8 and PW-ZOOM load spectra in photogrammetric flights was processed for two cases: entire flights (i.e., a manual take-off and landing plus an autonomic flight along the programmed photogrammetry path) and selected photogrammetry-only parts (i.e., flight controlled automatically by the autopilot). 10 X-8 flight logs and 23 PW-ZOOM flight logs were used for the analysis.

Figure 10 presents the charts representing LS envelopes and LS-weighted envelopes of entire flights of both X-8 and PW-ZOOM planes. As one can see, the range of load variations is nearly the same, but the differences of the numbers of load cycles per 1 h for the same case of curve exceed one order of magnitude. This means that the X-8 LS may produce higher fatigue wear (see next section). Figure 11 presents the same charts for the photogrammetric part of the flights only. In this case, there is a big difference in the range of load variation (i.e., the PW-ZOOM flies in a calmer way in terms of load oscillation range and number of load cycles).

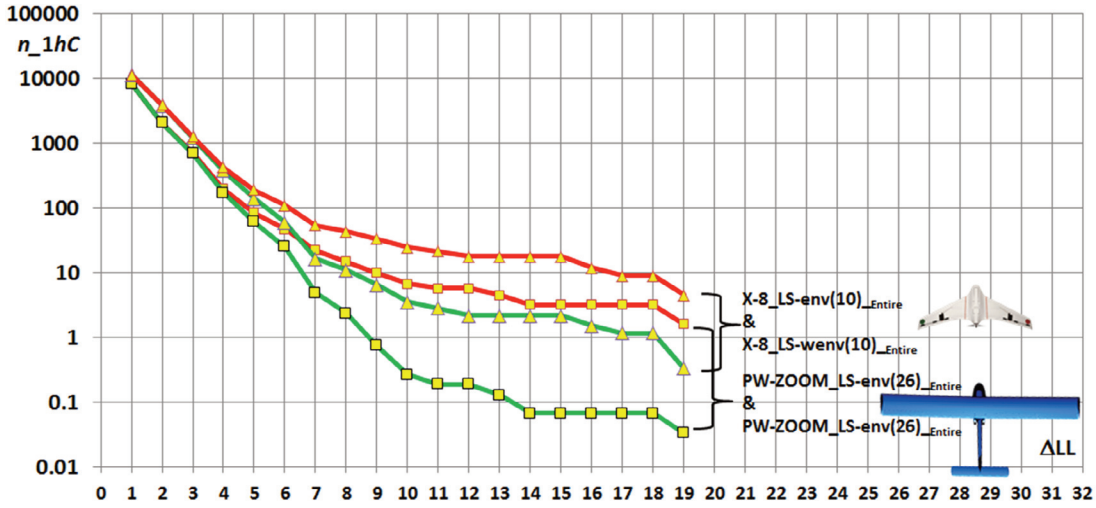


Figure 10. Comparison between LS envelopes and LS-weighted-envelopes of two UAVs (entire flights case).

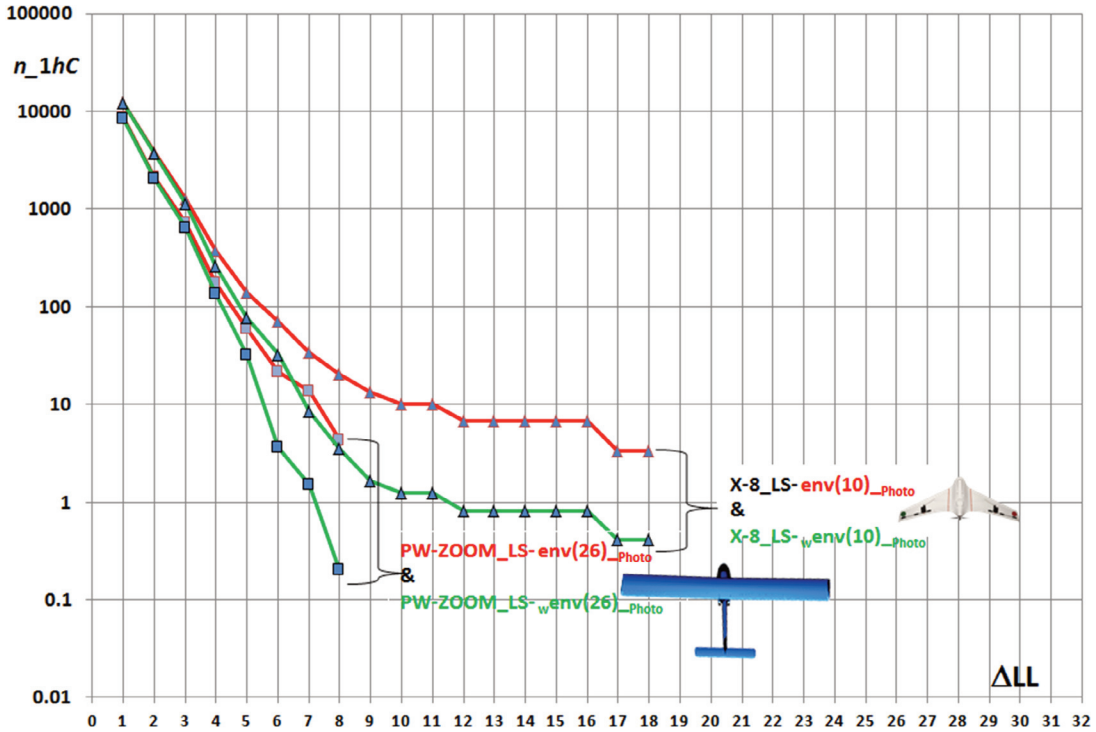


Figure 11. Comparison between LS envelopes and LS-weighted envelopes of two UAVs (photogrammetry part of flights case only).

Discussion of the reasons for large differences in the PW-ZOOM and X-8 load spectra

Fragments of the load spectra in which the number of load cycles per hour is in the range of 10^3 to 10^4 coincide with the range of small oscillations of acceleration resulting from the natural dynamic characteristics of the aircraft autopilot system. This means

that in addition to the traditional sources like gusts or maneuver, these characteristics affect the load factor variation.

An important dynamic feature of an aircraft designed for photogrammetric tasks is dynamic response to gust. The flight must be stable, and all oscillations caused by gusts should be effectively dumped.

In the case of "sharp edged" gusts (Leishman, 2022), the increase in the load factor can be described by the following formula:

$$\Delta n_z = \frac{\rho}{2} \cdot \frac{S}{Q} \cdot \frac{dC_l}{d\alpha} \cdot \eta \cdot w \cdot V \quad (10)$$

,

where ρ is air density, S is wings area, Q is aircraft mass, c_l is the lift force coefficient, is the angle of attack, w is the value of the vertical gust, V is current airspeed, and η is the gust mitigation factor.

The most important factors related to the plane are the wing loading and the $dC_l/d\alpha$ characteristic. To investigate the impact of the gust on both aircraft, calculations were carried out for gusts in the range 5 m/s to +5 m/s occurring at the cruising speeds of each aircraft (i.e., 70 km/h for X-8 and 100 km/h for PW-ZOOM). Due to the fact that the gust mitigation factor for the same gust value w may be different for both aircraft, the calculations were carried out for the whole range of variability of this parameter starting from 0.1 up to 1. The values of Δn_z were recalculated to the values of ΔLL.

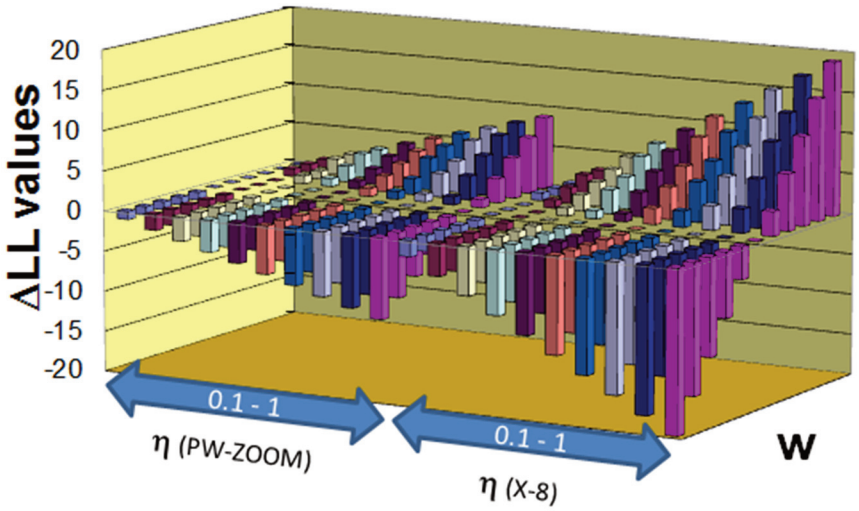


Figure 12. Comparison of ΔLL values induced by vertical gusts varying from 5m/s up to +5m/s.

Figure 12 shows that the influence of the gust is almost half of the PW-ZOOM case. This fact explains why the PW-ZOOM's LS is much milder than that in the X-8.

Comparison of the photo-points dispersion for PW-ZOOM and X-8 photogrammetric missions

The aim of this part of the work was to check whether the differences in the dynamic behavior of both planes resulting in different load spectra translate into differences in the quality of the material obtained during photogrammetric missions. The distribution of photo-points on the Earth's surface was adopted as a qualitative criterion because it is important for the orthophotomap production process. The term photo-point refers to the trace of intersection of the optical axis of the camera with the plane located at the height of 0-AGL (i.e., the take-off level). One PW-ZOOM flight and one X-8 flight were selected for the analysis. Both selected flights were performed in light wind to eliminate the possible influence of turbulence resulting from the flow around uneven terrain. The analysis procedure is explained for the X-8 flight (log20150630_121339). The flight altitude was 300 m. During flight, the optical axis of the camera was oscillating, as shown in Fig. 13.

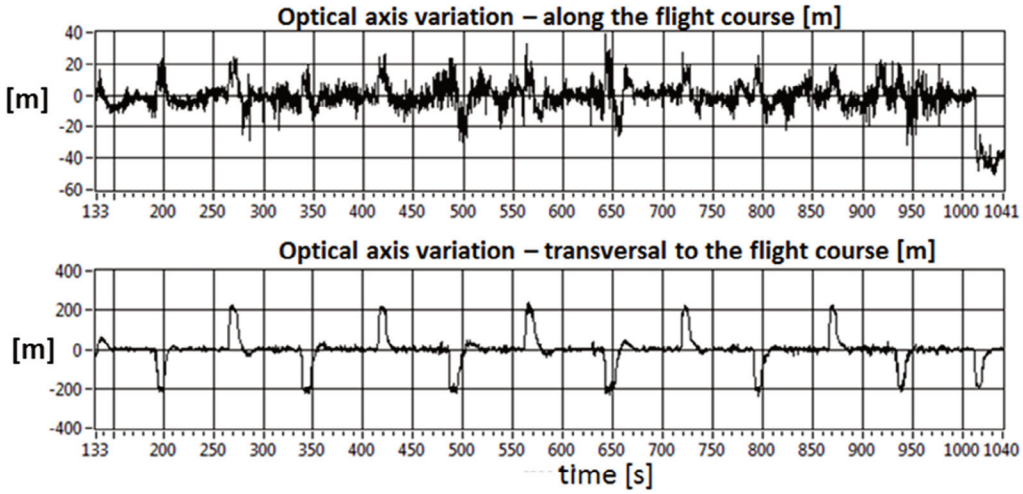


Figure 13. Movement of the intersection point of the optical axis of the camera with the 0-AGL surface relative to the current GPS position of the aircraft.

Photos were taken every 2 s during the flight, but only photos from the zone marked with a dashed line were selected for analysis (i.e., when X-8 flew straight along the programmed photogrammetric grid –see Fig. 14a and 14b). A two-step analysis process was applied: first, the distances between each two consecutive photo-points were calculated (Fig. 14c), and then the mean value and the standard deviation were determined for this set of distances. The standard deviation of distances between two consecutive photo-points was adopted as a measure of the photo-points dispersion. In the case of a very regular scattering of photo-points, the expected result would be close to zero. For the considered flight of X-8, the result is equal to **10.44 m**. The same process applied for the PW-ZOOM flight gave the result **7.05 m**. This means that the prediction that there is a relationship between the LS and the quality of the photogrammetric material has been confirmed, although this relationship is not as strong as one might expect looking at the ILS differences in Figs. 10 and 11.

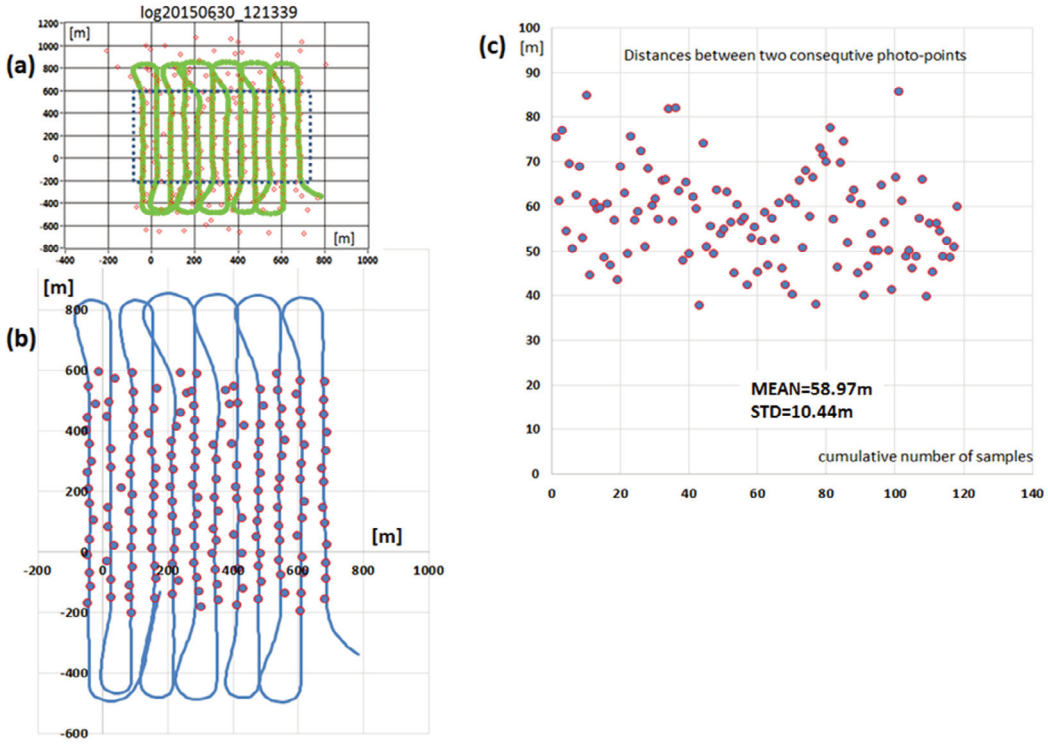


Figure 14. (a): GPS trajectory of the X-8 flight and the photo-points, (b) the zone of photo-points selected for analysis, (c) chart of distances, (d) chart of distance increments.

Comparison of the fatigue effect of the X-8 and the PW-ZOOM Load Spectra

The purpose of this section is to compare the fatigue effect of X-8 and PW-ZOOM load spectra applied to the same structural element. In these considerations, it does not matter what element it is and how it is loaded. Only its fatigue properties are important, i.e., the number of cycles to failure at a given amplitude of the load factor variation. The considerations are based on the Palmgren–Miner hypothesis, which is applied in the classic way (see Report AFS-120-73-2 issued by EMD 1973):

$$D = \sum_{i=1}^{l} \frac{n_i}{N_i} = 1, \tag{11}$$

where i is an index of constant amplitude load block; n is a number of cycles in the load block (defined here as a load cycles having the same ΔLL value), and N is the number of cycles to failure.

The following simplifying assumptions have been made:

1. The number of load cycles to failure depends only on the value of the load increment ΔLL. It means that the number of load cycles to failure is the same in the cells of the HC array that lie along the selected line parallel to the zero diagonal (see gray cells in the array presented in Fig. 3). In fact, the number of cycles to failure depends not only on the amplitude of the load cycle but also on

the mean value of the load cycle. However, for some structural materials, the isolines of the constant number of cycles to failure in the operating load range are near-parallel to this diagonal, which justifies the previous assumption.

2. The number of load cycles to failure is determined by the formula: $\log(N) = a \cdot \Delta LL + b$, where N is a number of load cycles to failure, a and b are the coefficients of linear equation, and their values are defined by the assumed values of $\log(N)$ for $\Delta LL = 1$ and $\Delta LL = 20$.
   Several combinations of those values were tested by the authors.

The evaluation of fatigue life was performed for two cases: the LS for entire flights and the LS for the photogrammetry part only. In each case, two approaches were adopted: conservative (using the LS envelope) and semi-conservative (using the weighted LS envelope). The synthetic results of the calculations are presented in the graph in Fig. 15.

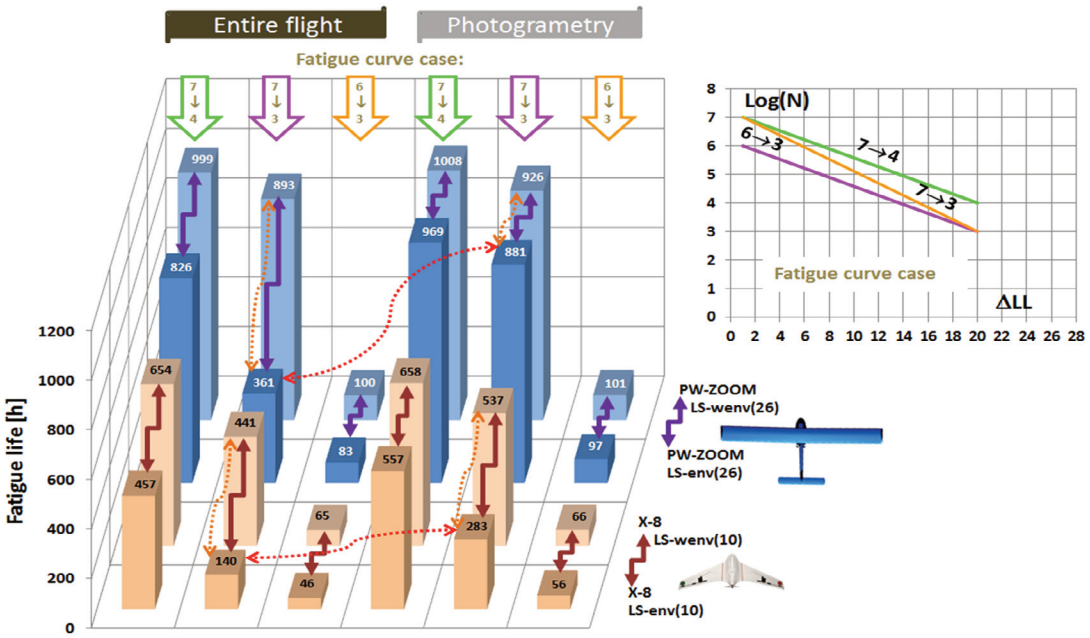


Figure 15. Estimated fatigue life vs type of UAV for the case of the entire flight or the photogrammetry part only, and vs three different fatigue characteristics of the critical structural element. LS, load spectrum; UAV, unmanned aerial vehicle.

As one can see, the fatigue characteristics of the material adopted for the calculations gave quite realistic results of fatigue life estimation.

- The milder LS of the PW-ZOOM leads to a much greater calculated fatigue life than that of the X-8 LS for all the considered fatigue characteristics. This concerns the results of both the analysis of the entire flights and the analysis of only photogrammetric parts.
- Deterioration of fatigue characteristics by 1 order causes the change in the fatigue life also by one order (see results for pink and green colors).
- The largest “forks” between the results of conservative and semi-conservative fatigue life calculations (i.e., based on the LS envelope and LS-weighted

envelope) occur for the steepest fatigue characteristics of tested structural element (see results for orange color).
- In the case of X-8, the differences in fatigue life resulting from the load spectra for entire flights and photogrammetry parts only are small. This is due to the fact that both load spectra are similar here (compare Figs. 10 and 11). It is completely different in the case of PW-ZOOM, where large differences in the load spectra were found in the flight with the manual control compared to the flight with the automatic control.

Summary and conclusions

- The normal and weighted LS envelopes are convenient tools for determining the range of load cycles variability between the semi-conservative approach (i.e., following the statistically influenced envelope of the worst load histories) and the conservative approach (i.e., following directly the envelope of the worst load histories) for a spectrum of loads representative for the conducted flight session.
- Comparative analysis of the X-8 and PW-ZOOM aircraft load spectra showed that the PW-ZOOM aircraft LS is much milder (despite the fact that the X-8 flights took place only in light winds over flat terrain, while the PW-ZOOM flights took place in a larger range of wind speeds over mountains and glaciers – in conditions conducive to turbulence).
- Although the cumulative number of load cycles for all possible load increments is comparable for both aircraft, the X-8 Ls has more cycles for large load increments. This translates into a greater fatigue effect.
- It has been shown that the differences in the load spectra translate into significant differences in the fatigue life of the structural element subjected to both load spectra.
- An important reason for the difference in load spectra is the different sensitivity of the two aircraft to gusts; the flying wing reacts more dynamically, causing acceleration and load factor oscillations.
- Oscillations of the load factor translate into small angular oscillations of the aircraft body, which, in turn, translates into the quality of photogrammetric images. In the absence of camera stabilization systems (which applies to both aircraft described here), this aspect is of great importance.

References

Engineering and Manufacturing Division, Airframe Branch. *Fatigue evaluation of wing and associated structure on small airplanes*, Report No. AFS-120-73-2, sponsored by Department of Transportation, Federal Aviation Administration, Washington, DC 1973.

Everaerts, J. (2008). The use of unmanned aerial vehicles (UAVS) for remote sensing and mapping, *The International Archives of the Photogrammetry, Remote Sensing and Spatial Information Sciences*. Vol. XXXVII. Part B1, 1187–1191.

Giordan, D., Adams, M.S., Aicardi, I., et al. (2020). The use of unmanned aerial vehicles (UAVs) for engineering geology applications. *Bulletin of Engineering Geology and the Environment*, *79*, 3437–3481.

Głowacki, D., & Rodzewicz, M. (2014). Investigation into Load Spectra of UAVS Aircraft. *Fatigue of Aircraft Structures*, *2013*(5), 40–52. https://doi.org/10.2478/fas-2013-0004

Goetzendorf-Grabowski, T., & Rodzewicz, M. (2016). Design of UAV for photogrammetric mission in Antarctic area. *Proceedings of the Institution of Mechanical Engineers, Part G: Journal of Aerospace Engineering*, *231*(9), 1660-1675. https://doi.org/10.1177/0954410016656881

Goetzendorf-Grabowski, T., Tarnowski, A., Figat, M., et al. (2021). Lightweight unmanned aerial vehicle for emergency medical service – Synthesis of the layout, *Proceedings of the Institution of Mechanical Engineers, Part G: Journal of Aerospace Engineering*, *235*(1), 5–21.

Gryte, K., Hann, R., Alam, M., Rohac, J., Johansen, T.A., & Fossen, T.I. (2018). Aerodynamic modeling of the Skywalker X8 Fixed-Wing Unmanned Aerial Vehicle. *2018 International Conference on Unmanned Aircraft Systems (ICUAS)*, 826–835. https://doi.org/10.1109/ICUAS.2018.8453370.

Jin, G. D., Lu, L. B., Gu, L. X., Liang, J., & Zhu, X. F. (2013). Fatigue Life of UAV Airframe Based on Damage Coefficient. In *Advanced Materials Research*, *709*, 358–362. https://doi.org/10.4028/www.scientific.net/amr.709.358

Kossira, H., & Reinke, W. (1986). *Entwicklung eines Belastungskollektivs fur leichte Motorflugzeuge aus den Beanspruchungsmessungen an einem Segelflugzeug*, IFL-IB 86-04, TU Braunschweig.

Kozera, C.A. (2018). Military Use of Unmanned Aerial Vehicles – A Historical Study, *Safety & Defence, 4*(1), 17–21. https://doi.org/10.37105/sd.4

Leishman, J. G. (2022). *Introduction to Aerospace Flight Vehicles*. https://doi.org/10.15394/eaglepub.2022.1066

Norasma, C., Fadzilah, M., Roslin, N., et al. (2019). Unmanned Aerial Vehicle Applications In Agriculture, *IOP Conference Series: Materials Science and Engineering 506*(1), 012063. https://doi.org/10.1088/1757-899X/506/1/012063

Rodzewicz, M., & Glowacki, D. (2020). Study of Load Spectrum Occurring in the Course of Photogrammetric Missions of the UAV. In: Niepokolczycki, A., Komorowski, J. (eds) *ICAF 2019 – Structural Integrity in the Age of Additive Manufacturing. ICAF 2019. Lecture Notes in Mechanical Engineering*. Springer, Cham. https://doi.org/10.1007/978-3-030-21503-3_88.

Rodzewicz, M., Głowacki, D., & Hajduk, J. (2017). Some dynamic aspects of photogrammetry missions performed by "PW-ZOOM" – The UAV of Warsaw University of Technology, *Archive of Mechanical Engineering*, *64*(1), 37–55. https://doi.org/10.1515/meceng-2017-0003

Rodzewicz, M. (2012). Airworthiness tests of the UAV structure – fatigue issues. *Fatigue of Aircraft Structures*, 2012(1), 82–93.

Rodzewicz, M. (2023). Close-proximity, conservative extrapolation of load spectra. *Aircraft Engineering and Aerospace Technology*, 95(11), 1–13. https://doi.org/10.1108/AEAT-12-2021-0374.

Slack, A.J. (2013). Sorces: Military Robots and Drones: A Reference Handbook. *Reference & User Services Quarterly*, *3*(1), 88–89. https://doi.org/10.5860/rusq.53n1.88b

Zmarz, A., Rodzewicz, M., Dąbski, M., et al. (2018). Application of UAV BVLOS remote sensing data for multi-faceted analysis of Antarctic ecosystem. *Remote Sensing of Environment*, *217*, 375–388. https://doi.org/10.1016/j.rse.2018.08.031